Department of Mechanical Engineering
University of Wisconsin--Milwaukee
Milwaukee, Wisconsin 53201

A STUDY OF THE SECOND AND THIRD ORDER CLOSURE MODELS OF TURBULENCE FOR PREDICTION OF SEPARATED SHEAR FLOWS

August 1985

by

R. S. Amano
Principal Investigator

The report documents research completed during the period of January 15 thru July 15, 1985 under NASA-Lewis Research Grant No. NAG 3-546.

TF/85/8

222E/2241E

ABSTRACT

The hybrid model of the Reynolds-stress turbulence closure, which was developed in the earlier work of this project, is tested for the computation of the flows over a step and disk. Here it is attempted to improve the redistributive action of the turbulence energy among the Reynolds stresses. By evaluating the existing models for the pressure-strain correlation, better coefficients are obtained for the prediction of separating shear flows. Furthermore, the diffusion rate of the Reynolds stresses is reevaluated adopting several algebraic correlations for the triple-velocity products. The models of Cormack et al., Daly-Harlow, Hanjalic-Launder, and Shir were tested for the reattaching shear flows. It was generally observed that all these algebraic models give considerably low values of the triple-velocity products. This is attributed to the fact that none of the algebraic models can take the convective effect of the triple-velocity products into account in the separating shear flows, thus resulting in much lower diffusion rate than Reynolds stresses. In order to improve the evaluation of these quantities correction factors are introduced based on the comparison with some experimental data.

TABLE OF CONTENTS

ABSTRACT 1

TABLE OF CONTENTS ii

NOMENCLATURE iii

1. INTRODUCTION 1

2. MATHEMATICAL FORMULATION 3

2.1 Reynolds-Stress Equations 3
2.2 Pressure-Strain Correlations 4
2.3 Third-Order Closure Model 7

3. NUMERICAL MODEL 9

3.1 Numerical Method 9
3.2 Boundary Conditions 9

4. RESULTS AND DISCUSSION 11

4.1 Flow Beyond a Disk (Evaluation of Pressure-Strain Correlations). 11
4.2 Flow Beyond a Step (Evaluation of the Triple-Velocity. 14
Correlations)

5. SUMMARIZING REMARKS 17

6. REFERENCES 20

7. FIGURES 22

NOMENCLATURE

$a_1, a_2, a_3, a_4 a_5, a_6$	constants used in pressure-strain correlations
$b_1, b_2,$	constants used in pressure-strain correlations
C_1, C_p, C_ϕ	coefficients used in turbulence model
$C^{\dagger}_{jk\ell}$	coefficient tensor
D_c	diameter of the cylinder
D_d	diameter of the disk
D_{ij}	diffusion of $\overline{u_i u_j}$
G	generation of turbulence kinetic energy
G_{ij}	generation of Reynolds stresses
H	step height
k	turbulence kinetic energy
p	pressure fluctuation
P	mean pressure
Q_{ij}	generation rate used in pressure-strain correlation
r	radial coordinate
R	radius of the disk
u	fluctuating velocity
U	mean velocity
U_{IN}	mean velocity at the inlet
U_∞	free stream velocity
v	fluctuating velocity in y-direction
V	mean velocity in y-direction
x	Cartesian coordinate
y	Cartesian coordinate
Y_o	height of inlet flow section
α_i	coefficient used in Eq. (22)

δ_{ij}	Kronecker delta
ϵ	energy dissipation rate
μ	dynamic molecular viscosity
ρ	density
Φ_{ij}	pressure-strain correlation

Subscripts

i, j, k, ℓ, m	tensor notations

1. INTRODUCTION

This report summarizes the study of the behavior of the second- and third-moments in the wake region behind bodies. The flow in such a situation has been investigated by formulating the transport equations for the kinematic Reynolds stresses $\overline{u_i u_j}$.[1] In evaluating the Reynolds stresses in the shear region it is important to understand the mechanism of energy transfer which occurs among the Reynolds-stress components. Separated flow generates turbulence resulting in an increase in the heat and mass transfer rates which could be advantageous in some cases and, therefore, preferable (e.g., internal combustion engines). On the other hand, separation causes pressure losses which are undesirable but are sometimes difficult to avoid in aeronautics. Whether it is required to create, control or avoid separation and recirculation, a better understanding of the turbulence phenomena in the situation will provide a good basis for attempts to improve the performance of fluid machinery which operates creating such separating turbulent flows.

The recent development of computer techniques for solving the partial differential equations governing these flows has made theoretical studies easier and less costly by eliminating the need for extensive experimental work during design stages.

A model of the Reynolds stresses was first proposed by Rotta[2], and has been developed and improved by a number of researchers.[3-8] The correlation of pressure-strain was proposed by Naot et al.[4-6] and Launder et al.[8] Naot et al. evaluated the pressure-strain correlation term by integrating over space after inserting two-point correlation functions, whereas Launder et al. obtained the results by assuming a fourth-order tensor consisting of linear Reynolds-stress elements. As a simplified model of the Reynolds-stress

closure, an algebraic stress model which does not possess both convection and diffusion terms was developed in a similar manner by Rodi.[9]

In the authors' previous paper[10] several proposed closures for the Reynolds-stress model were tested for heat transfer characteristics along the walls of axisymmetric sudden expansion pipes. After the computation with several different models, it was found that the pressure-strain correlation proposed by Launder et al.[8] showed slightly better agreement with experimental data for Nusselt number distributions along the pipe walls than with other models. Moreover, incorporation of the wall correction terms in the pressure-strain also improved predictions by about 5 to 10 percent.

Here computations of the turbulent flow are made in the region beyond a disk by employing the second-order closure model of turbulence. The results are compared with the existing experimental data at several different steamwise locations.

Particular attention is paid to the evaluation of the pressure-strain correlation which plays an important role in transfering turbulence energy among the Reynolds-stress components in the separated shear flow region. First, the models of Naot et al.[4-6] and Launder et al.[8] are examined, and the results computed using these models are compared with existing experimental data. Moreover, a simpler model is formulated that provides better profiles of the Reynolds stresses in the wake region.

The study is further extended to the evaluation of the diffusion action of the Reynolds stress. As was discussed in the previous report,[11] the change in the triple-velocity products is significantly large in the wake region resulting in a considerable variation in the diffusion rate of the Reynolds stresses. Thus, it is important to reevaluate the existing models of

the third-order closure for better understanding of such diffusion processes in the separated shear layers. In the present report four models of the third-order closure are examined, and the results are compared with the experimental data of Chandrsuda and Bradshaw.[12] The models considered are those proposed by Daly and Harlow,[3] Hanjalic and Launder,[13] Shir,[14] and Cormack et al.[15] Mathematical formulations, along with the results and discussion, are presented in subsequent sections.

2. MATHEMATICAL FORMULATION

The steady, two-dimensional form of continuity and momentum equations are given as:

Continuity Equation:

$$\frac{\partial}{\partial x_j}(\rho U_j) = 0 \tag{1}$$

Momentum Equation:

$$\frac{\partial}{\partial x_j}(\rho U_i U_j) = -\frac{\partial P}{\partial x_i} + \frac{\partial}{\partial x_j}[\mu(\frac{\partial U_i}{\partial x_j} + \frac{\partial U_j}{\partial x_i}) - \rho\overline{u_i u_j}] \tag{2}$$

2.1 Reynolds-Stress Equations

The transport equations for the Reynolds stresses are given as

$$\frac{\partial}{\partial x_k}(U_k\overline{u_i u_j}) = G_{ij} - \varepsilon_{ij} + \phi_{ij} + \phi_{ij,w} + D_{ij} \tag{3}$$

where

$$G_{ij} = -(\overline{u_j u_k}\frac{\partial U_i}{\partial x_k} + \overline{u_i u_k}\frac{\partial U_j}{\partial x_k}) \quad : \text{ generation} \tag{4}$$

$$\varepsilon_{ij} = 2\nu \overline{\frac{\partial u_i}{\partial x_k} \frac{\partial u_j}{\partial x_k}} \quad : \text{ dissipation} \tag{5}$$

$$\phi_{ij} = \overline{\frac{p}{\rho} \left(\frac{\partial u_i}{\partial x_j} + \frac{\partial u_j}{\partial x_i}\right)} \quad : \text{ pressure-strain correlation} \tag{6}$$

and

$$D_{ij} = - \frac{\partial}{\partial x_k} \left(\overline{u_i u_j u_k}\right) \quad : \text{ diffusion} \tag{7}$$

Equation (5) was approximated by the form given by Rotta[2] as:

$$\varepsilon_{ij} = \frac{2}{3} \delta_{ij} \varepsilon \tag{8}$$

2.2 Pressure-Strain Correlations

Several models have been proposed for the pressure-strain correlations, but these have been tested only for relatively simple flows such as free shear flows and boundary layers. To date, these have not yet been extensively tested for the recirculating flows. In this report three models are employed to compute all turbulent kinematic stress components.

Model 1: Naot et al.[4]

$$\overline{\frac{p}{\rho} \left(\frac{\partial u_i}{\partial x_j} + \frac{\partial u_j}{\partial x_i}\right)} = - C_\phi \left(G_{ij} - \frac{2}{3} \delta_{ij} G\right) + \phi \tag{9}$$

Model 2: Naot et al.[6]

$$\overline{\frac{p}{\rho}\left(\frac{\partial u_i}{\partial x_j}+\frac{\partial u_j}{\partial x_i}\right)} = -a_1\left(G_{ij}-\frac{2}{3}\delta_{ij}G\right)+a_2\left(Q_{ij}-\frac{2}{3}\delta_{ij}G\right)$$

$$+a_3 k\left(\frac{\partial U_i}{\partial x_j}+\frac{\partial U_j}{\partial x_i}\right)+\phi \qquad (10)$$

Model 3: Launder et al.[8]

$$\overline{\frac{p}{\rho}\left(\frac{\partial u_i}{\partial x_j}+\frac{\partial u_j}{\partial x_i}\right)} = -a_4\left(G_{ij}-\frac{2}{3}\delta_{ij}G\right)-a_5\left(Q_{ij}-\frac{2}{3}\delta_{ij}G\right)$$

$$-a_6 k\left(\frac{\partial U_i}{\partial x_j}+\frac{\partial U_j}{\partial x_i}\right)+\phi \qquad (11)$$

where

$$G = -\overline{u_i u_j}\frac{\partial U_i}{\partial x_j} \qquad (12)$$

$$Q_{ij} = -\left(\overline{u_i u_k}\frac{\partial U_k}{\partial x_j}+\overline{u_j u_k}\frac{\partial U_k}{\partial x_i}\right) \qquad (13)$$

$$\phi = -C_1\frac{\epsilon}{k}\left(\overline{u_i u_j}-\frac{2}{3}\delta_{ij}k\right) \qquad (14)$$

and where $C_1 = 1.5$.

The coefficients used above are given as

$$a_1 = (76 - 8\ b_1)/105$$

$$a_2 = (22 + 64\ b_1)/105$$

$$a_3 = 2\ (9 + 72\ b_1)/315 \qquad (15)$$

$$a_4 = (b_2 + 8)/11$$

$$a_5 = (8\ b_2 - 2)/11$$

$$a_6 = (30\ b_2 - 2)/55$$

The first model was developed by removing the isotropic constraint from the double velocity two-point correlation tensor. The second model, an extension of the first, was proposed in terms of the single point tensor and three arbitrary functions of the absolute value of the two-point separation distance. In this model the value of b_1 was determined as

$$b_1 = \int_0^\infty \frac{K(r)}{r}\, dr \qquad (16)$$

where

$$K(r) = C^+_{2211} - C^+_{1122} \qquad (17)$$

and where $C^+_{jk\ell m}$ represents the coefficient tensor that is used to correlate between the single-point double-velocity and the two-point double-velocity products such as

$$\overline{u_j(x)\ u_k(x+r)} = C_{jk\ell m}\ (x,r)\ \overline{u_\ell(x)\ u_m(x)} \qquad (18)$$

The third model was obtained by approximating the pressure-strain correlation by an arbitrary fourth-order tensor where the single-point double-velocity correlations were used.

2.3 Third-Order Closure Model

As is discussed in the last part of the introduction section, the triple velocity fluctuation products, $\overline{u_i u_j u_k}$, should be evaluated appropriately in a separating and reattaching flow region. Here the four existing models of the third-order closure, all in algebraic forms, are reviewed and tested for the reattaching shear layers. These models are summarized in this section.

Daly and Harlow[3] obtained an algebraic expression with a simplification of such a transport equation of $\overline{u_i u_j u_k}$ as follows

$$\overline{u_i u_j u_k} = - 2.0\, C_p \frac{k}{\varepsilon} \overline{u_k u_\ell} \frac{\partial \overline{u_i u_j}}{\partial x_\ell} \tag{19}$$

Hanjalic and Launder[13] obtained the following algebraic equation.

$$\overline{u_i u_j u_k} = - 0.08\, C_p \frac{k}{\varepsilon} \left[\overline{u_i u_\ell} \frac{\partial \overline{u_j u_k}}{\partial x_\ell} + \overline{u_j u_\ell} \frac{\partial \overline{u_k u_i}}{\partial x_\ell} + \overline{u_k u_\ell} \frac{\partial \overline{u_i u_j}}{\partial x_\ell}\right] \tag{20}$$

Shir[14] proposed the following expression by approximating the first Reynolds stress that appears in Eq. (19) to be isotropic.

$$\overline{u_i u_j u_k} = - 0.04\, C_p \frac{k^2}{\varepsilon} \frac{\partial \overline{u_i u_j}}{\partial x_k} \tag{21}$$

Cormack et al.[15] obtained algebraic expressions by approximating the experimentally determined profiles for $\overline{u_i u_j}$, ε and $\overline{u_i u_j u_k}$ with a

polynomial with coefficients chosen to give a least-square fit to the data and discretized the cross-stream coordinate in each flow by using the most general model for the triple velocity correlation tensor as generated using the asymptotic approach of Lumley and Khajeh Nouri.[7] The model they obtained is as follows:

$$\overline{u_i u_j u_k} = \frac{4k^2}{\varepsilon} C_p \{2\alpha_1 (\delta_{ij}\delta_{k\ell} + \delta_{ik}\delta_{j\ell} + \delta_{kj}\delta_{i\ell}) \frac{\partial k}{\partial x_\ell} + \alpha_2 (\frac{\partial a_{ik}}{\partial x_j} + \frac{\partial a_{ij}}{\partial x_k} + \frac{\partial a_{kj}}{\partial x_i})\} + \frac{2k}{\varepsilon} \{2\alpha_3 (\delta_{ik}a_{j\ell} + \delta_{ij}a_{k\ell} + \delta_{j\ell}a_{i\ell}) \frac{\partial k}{\partial x_\ell} + \alpha_4 (a_{ik}\frac{\partial a_{j\ell}}{\partial x_\ell} + a_{ij}\frac{\partial a_{k\ell}}{\partial x_\ell} + a_{kj}\frac{\partial a_{i\ell}}{\partial x_\ell})\} \quad (22)$$

where

$$a_{ij} = \overline{u_i u_j} - \frac{2}{3} k\delta_{ij} \quad (23)$$

Out of the twenty parameters, α_i, that they had started out with, they were able to determine and optimize the most significant four coefficients. The values of these parameters have been recommended for various kinds of flows along with the universal value applicable to most of the flows.

$$\begin{aligned} \alpha_1 &= -8.14 \times 10^{-3} \\ \alpha_2 &= -1.72 \times 10^{-2} \\ \alpha_3 &= -4.80 \times 10^{-3} \\ \alpha_4 &= -0.102 \end{aligned} \quad (24)$$

In the original forms of Eqs. (19)-(22), the coefficient C_p is unity, but the best values for C_p were investigated for the reattaching shear flows by comparison with experimental data. The recommended values are given in Sec. 4.2.

3. NUMERICAL MODEL

3.1 Numerical Method

The solution method of the transport equations described in the preceding section is the same finite volume method as the one used in [1] in which the differencing scheme is the modified hybrid scheme of Amano.[16] This scheme has a combined mode of convection and diffusion which is derived by expanding the analytical one-dimensional solution up to the fourth-order term. The cell structure for mean-velocity components is the staggered system in which the locations of the mean velocities U and V are a half-cell shifted in x- and y-directions, respectively. All the normal Reynolds stresses ($\overline{u_i^2}$) are evaluated at the scalar node point along with P, k and ε. However, the shear Reynolds stress ($\overline{uv}$) is located at the southwest corner of the scalar cell. This is because the main driving strains for the shear stress are $\partial U/\partial y$ and $\partial V/\partial x$ which can easily be evaluated without any interpolations (Fig. 1).

3.2 Boundary Conditions

For the examination of the pressure-strain correlation, a cylindrical coordinate was used since all the components of the Reynolds stresses ($\overline{u^2}$, $\overline{v^2}$, $\overline{w^2}$, and $\overline{uv}$) for two-dimensional problems can be investigated instead of just two components of normal stresses ($\overline{u^2}$ and $\overline{v^2}$) and the shear component ($\overline{uv}$). The flow domain is shown in Fig. 2. For the investigation of

the triple-velocity products, however, the plane two-dimensional coordinate was employed due to the limitation of the experimental data for these quantities. (see Fig. 3)

There are three different types of boundary conditions to be specified for the computation of the flows in Figs. 2 and 3: inlet, outlet, and wall boundary conditions. At the inlet all the quantities are specified according to the fully developed condition. At the outlet a continuative flow condition is applied where gradients of flow properties in the flow direction are zero (Neumann conditions), i.e., $\partial\phi/\partial x = 0$, where $\phi = U_i$, k, ϵ, $\overline{u_i u_j}$, etc. This outlet is located about 80-120H downstream from the step so that its influence on the main flow region is negligibly small.

At the wall boundaries the velocities and turbulence quantities must be specified functionally according to the law of the wall. The velocity component normal to the wall is simply set as zero. The wall boundary values for k are determined by means of wall functions based on the assumption of a logarithmic near-wall velocity distribution which allows the wall-shear stress to be extracted from the "log law" and the value of velocity parallel to the wall to be computed along the grid line closest to the wall. The energy dissipation rate, ϵ, is evaluated under local equilibrium condition. Near-wall effects on the turbulence structure, associated with steep velocity variations, are also taken into account by introducing appropriate modifications to the generation and dissipation of the turbulence energy and the energy dissipation rate for the finite volume adjacent to the wall.[16]

The boundary values for the Reynolds stresses are determined as

$$\overline{u^2} = 1.21k$$

$$\overline{v^2} = 0.24k \qquad (25)$$

$$\overline{w^2} = 0.55k$$

$$\overline{-uv} = -0.24k + \frac{\nu}{\rho}\frac{dP}{dx}$$

in the wall adjacent numerical cells. The details of the derivation of (25) is given in ref. [11].

4. RESULTS AND DISCUSSION

4.1 Flow Beyond a Disk (Evaluation of Pressure-Strain Correlations)

The flow field considered here is shown in Fig. 2. The diameter of the cylinder is 1/3 of the disk diameter. The computational domain is subdivided into many control volumes in such a way that the sizes increase at the rate of 2 ~ 3 % in both x and r directions. In this way the size of the numerical control volume is reasonably fine in the recirculating region but is relatively coarse in both the outer region and the downstream region where flows are mainly parabolic.

Several cases with different mesh sizes were tested and the size of 42 x 42 demonstrated a grid independent state for the flow domain consisting of four radii of the disk in height and twenty radii in length.

Figure 4 demonstrates the axial velocity profiles at several different locations behind the disk. Agreement between computed results and the experimental data of Smyth[17] is very good (within 15% discrepancy). It was also

discerned that the velocity profiles were almost independent of the pressure-strain correlation although the computed velocity profiles using all the models are not shown in the figure.

Figure 5 shows the normal stress profiles of $\overline{u^2}$ and $\overline{v^2}$ at four different locations downstream of the disk. The computations were made by using Models 1, 2 and 3 as defined in Sec. 2.2, and the results were compared with the experimental data of Smyth.[17] When the coefficient $C_\phi = 2/3$ is used for Model 1 (which was recommended by the originators[4]), the results are all similar to each other. This is mainly because, although all the models are derived differently, their final forms are very close. In particular, Models 2 and 3 have almost the same values for the coefficient of the first terms on the right-hand side of both Eqs. (10) and (11). Naot et al.[6] obtained the value of -0.5 for the coefficient b_1 and Launder et al.[8] chose the value 0.4 for b_2 which results in $a_1 = a_4 = 0.76$. Also, it is noticed that the second and the third terms of Models 2 and 3 have a minor influence on the levels of turbulence stresses; thus, the pressure-strain correlation may be represented by the first term alone. Note that Model 1 has this term only.

In Fig. 5 the computed results using Model 1 with $C_\phi = 0.4$ are also shown. This value was recommended by Launder et al.[8] in reference to equilibrium shear flows. The computed results using the coefficient $C_\phi = 0.4$ show that the levels of $\overline{u^2}$ increase about 20% while those of $\overline{v^2}$ decrease about the same amount; this indicates that the redistributive action is reduced by about 20% by changing C_ϕ from 0.667 to 0.4. Therefore, the turbulence energy created due to mean strain of the main stream flow ($\overline{u^2}$) is not transferred completely to the normal components ($\overline{v^2}$ and $\overline{w^2}$) of the turbulence stresses.

It was generally observed that all the models underpredict the levels of the Reynolds stresses by 10-50%. In order to predict the Reynolds stresses more accurately in recirculating flows, the original models tested for equilibrium shear flows need to be revised. For ease of analysis Model 1 was chosen to refine prediction of the turbulence level. Two computations were performed by using values of 0.2 and 1.2 for C_ϕ. The results are shown in Fig. 6. As is depicted in this figure, the small value of coefficient C_ϕ results in appropriate levels of $\overline{u^2}$ but unacceptably low levels of $\overline{v^2}$. On the other hand, the large value of C_ϕ gives reversed results; that is, the levels of $\overline{v^2}$ are substantially high but those of $\overline{u^2}$ are too low.

When the flow reattaches on the center cylinder, the flow starts accelerating in the downstream direction which causes a high mean normal strain as the flow recovers. Thus, the term with $\overline{u^2}\,\partial U/\partial x$ in the pressure-strain correlation in the $\overline{u^2}$-equation becomes higher than those in the fully developed flows which results in significant energy transfer from $\overline{u^2}$ to $\overline{v^2}$. This effect must be suppressed to some extent in the present flow situation, whereas the corresponding component which balances the energy level of $\overline{v^2}$ is relatively small. Therefore, the redistributive action in the $\overline{v^2}$ equation needs to be promoted more.

For the reasons discussed above, the case when the coefficient C_ϕ for $\overline{u^2}$ was decreased to 0.2 and when that for $\overline{v^2}$ was raised to 1.2 is demonstrated in the same figure. The results obtained with this treatment show a large improvement (see Fig. 6). This observation suggests that the coefficients of the isotropic generation rates for the Reynolds stresses (i.e. the first terms of Eqs. (9) - (11)) should be adjusted by their values by the strength of the mean strains, since the flow patterns are strongly affected by

the mean strains. The strain variations are particularly complex in reattaching shear layers being accompanied by recirculating flows. In this way the Reynolds stresses can be more accurately evaluated by using such simpler formulations.

In Fig. 7 all the Reynolds stresses computed using the method mentioned above are displayed at several different axial locations.

4.2 Flow Beyond a Step (Evaluation of the Triple-Velocity Correlations)

Before computing the triple-velocity products in the region behind a step, each component of the Reynolds stress equation (3) was solved along with the momentum, turbulence energy, and turbulence energy dissipation rate equations.

To establish an optimum grid system, exploratory grid tests were performed using 32x32, 42x42 and 52x52 mesh sizes and several different grid expanding factors in the downstream direction. Because computations with coarse mesh sizes fail to provide a decipherable trend in the Reynolds stress distributions and because the triple-velocity products vary steeply in the shear layer region the mesh size of 52x52 was used with an axial length of 50 step heights for a step ratio of $Y_0/H = 2.5$. The grid expansion factors used in the streamwise and transverse directions were 1.01 and 1.02, respectively.

Figure 8 shows the velocity profiles at two different locations behind the step. The results are compared with the experimental data of Chandrsuda and Bradshaw[12] obtained with two measurement techniques: a hot-wire, and a pressure-probe. Although slight disagreement appears near the wall at $x/H = 5.4$, the computed results are within 20% of the experimental data.

Figure 9 shows the normal Reynolds stresses ($\overline{u^2}$ and $\overline{v^2}$) and the shear Reynolds stress ($\overline{uv}$) distributions at three different locations in the flow field beyond a step. As is shown in this figure all the Reynolds stresses decay in the region downstream of the reattachment. In general, agreement between the computed results and the experimental data is fairly good. Based upon this agreement with the experimental data, the values of these Reynolds stresses were used to evaluate the algebraic models of the triple-velocity correlations (Eqs. (19) - (22)).

Figure 10 represents the distribution of the triple-velocity products at four different locations in the reattaching shear layer. It is commonly observed that all the models underpredict the levels of triple-velocity products everywhere. While the model of Shir consistently gives low levels, the model of Cormack et al. gives the highest levels for $\overline{uvv}$ and $\overline{vvv}$. The model of Daly-Harlow, which is most frequently used gives relatively lower levels except for $\overline{uuv}$, whereas the model of Hanjalic-Launder gives reasonably high levels for every component of the triple-velocity products.

In order to adjust for the discrepancy in the peak values of the triple-velocity products, the multiplying factor C_p in Eqs. (19) - (22) was incorporated to suitably compensate for the difference in the levels. This was done by dividing the experimental peak values of $\overline{u_i u_j u_k}$ by those predicted by the particular algebraic model. These factors were obtained for $\overline{uuv}$, $\overline{uvv}$, and $\overline{vvv}$ profiles at x/H locations of 6.4, 8.4, 10.3, and 12.3 for all four algebraic models.

Table 1 shows the values of these factors for individual components and models. The overall factor for a particular model is then obtained by averaging all the values of C_p for all the components of $\overline{u_i u_j u_k}$ for that model.

Table 1. Correction Factors for $\overline{u_i u_j u_k}$ for Different Algebraic Models

Models \ C_p	$\overline{uuv}$	$\overline{vvv}$	$\overline{uvv}$	Overall Average
Daly-Harlow	2.66	4.93	6.45	4.68
Hanjalic-Launder	4.18	3.74	4.76	4.22
Shir	7.68	14.20	18.66	13.51
Cormack et al.	-	2.12	3.52	2.82

The triple-velocity products were recomputed by using the overall averaged factors and the results are shown in Fig. 11. It is interesting to note that the peak values obtained by using the model of Hanjalic-Launder agree with the experimental data for all the components, whereas those obtained by other models agree with the experimental data only for $\overline{uvv}$ component. This indicates that, although the levels of the triple-velocity products can easily be adjusted according to flow conditions, we cannot necessarily obtain universally improved results for every component of $\overline{u_i u_j u_k}$ when using models other than that of Hanjalic-Launder.

The reason that the model of Hanjalic-Launder gives better results for all the components of $\overline{u_i u_j u_k}$ is because in the derivation process of this model the generation rates due to turbulence stresses as well as the diffusion rates of $\overline{u_i u_j u_k}$ were taken into account, even though the convection and the generation rates due to mean strains were neglected (see ref. 13). The generation caused by the stresses is particularly significant in the reattaching shear layer.

Unlike this model the models of Daly-Harlow and Shir do not include non-homogeneous flow effects. That is, when the Shir model, for example, is used, the transverse gradient of $\overline{u^2}$ is the only component that evaluates the behavior of the triple-velocity product, $\overline{uuv}$, in the transport equation of $\overline{u^2}$. The model of Daly-Harlow has an additional component that accounts for the variation of $\overline{u^2}$ in the streamwise direction for the corresponding product. However, these two models are notably limited in comparison with the Hanjalic-Launder model which accounts for variations of the shear stress in both directions in addition to the $\overline{u^2}$ variations. It should, however, be noted that all the models would produce similar results in an isotropic turbulence flow field.

The model of Cormack et al. was evaluated only for $\overline{vvv}$ and $\overline{uvv}$ since the values computed for $\overline{uuv}$ using its original form were not high enough to estimate the factor C_p within a reasonable range (see Fig. 10).

Finally, the triple-velocity products were recomputed by employing the individual correction factor C_p for each component and the results are shown in Fig. 12. In this case all the models agree with each other due to their component-wise correction factors.

5. SUMMARIZING REMARKS

Pressure-Strain Correlations

1. The models by Naot et al [6] and Launder et al.[8] effectively give similar results and both models are reasonably reliable.
2. The energy redistribution can be improved for reattaching shear flows by taking the effects of mean strain into account.

Triple-Velocity Correlations

1. The triple-velocity products need to be predicted accurately in the reattaching shear layer in order to evaluate the diffusion process of the Reynolds stress appropriately. The behavior of the triple-velocity products in such a complex turbulent flow is different from that in simpler flows.
2. All the existing algebraic models for the triple-velocity products underpredict the levels of $\overline{u_i u_j u_k}$ in the reattaching shear layer. The predicted levels can easily be improved by using a correction factor.
3. With the exception of the model of Hanjalic-Launder, all models cannot improve the prediction simply by employing a single value for C_p. Thus, it is difficult to obtain a unique value for the correction factor. This is because the Hanjalic-Launder model is the only one that includes the generation terms due to Reynolds stresses.

Finally, it was observed that none of the above models accurately predicts the overall levels of the triple-velocity products. This is primarily attributed to the fact that the convection effect of the triple-velocity products is never taken into account. This effect may be small in simple shear layers but is significant when the shear layer reattaches on a solid wall transfering high convective rates of $\overline{u_i u_j u_k}$ into turbulance diffusive energy near the wall and, subsequently, these high levels are transported in the downstream direction. In consequence, a model that can take into account this process must be developed and tested for complex turbulent flows.

6. REFERENCES

1. Amano, R. S. and Goel, P., "Computations of Turbulent Flow Beyond Backward-Facing Steps by Using Reynolds-Stress Closure," AIAA Journal, Vol. 23, No. 9, 1985, pp. 1356-1361.

2. Rotta, J. C., "Statistische Theorie Nichthomogener Turbulenz," Zeitschrift fur Physik, Vol. 129, 1951, pp. 547-572.

3. Daly, B. J. and Harlow, F. H., "Transport Equations of Turbulence," The Physics of Fluids, Vol. 13, No. 11, 1970, pp. 2634-2649.

4. Naot, D., Shavit, A., and Wolfshtein, M., "Interaction Between Components of the Turbulent Velocity Correlation Tensor Due to Pressure Fluctuations," Israel Journal of Technology, Vol. 8, No. 3, 1970, pp. 259-269.

5. Naot, D., Shavit, A., and Wolfshtein, M., "On the Two-Point Double-Velocity Correlation Tensor," Israel Journal of Technology, Vol. 9, Nos. 1-2, 1971, pp. 83-91.

6. Naot, D., Shavit, A., and Wolfshtein, M., "Two-Point Correlation Model and the Redistribution of Reynolds Stresses," The Physics of Fluids, Vol. 16, No. 6, 1973, pp. 738-743.

7. Lumley, J. L. and Khajeh Nouri, B., "Computational Modeling of Turbulent Transport," Advances in Geophysics, Vol. 18A, 1974, pp. 169-192.

8. Launder, B. E., Reece, G. J. and Rodi, W., "Progress in the Development of a Reynolds-stress Turbulence Closure," Journal of Fluid Mechanics, Vol 68, 1975, pp. 537-566.

9. Rodi, W., "The Prediction of Free Boundary Layers by Use of a Two-Equation Model of Turbulence," Ph.D. Thesis, University of London, Dec. 1972.

10. Amano, R. S. and Goel, P., "A Numerical Study of a Separating and Reattaching Flow by Using Reynolds-stress Turbulence Closure," Numerical Heat Transfer, Vol. 7, No. 3, 1984, pp. 343-357.

11. Amano, R. S. and Goel, P., "A Study of Reynolds-stress Closure Model," NASA-CR-174342, 1985.

12. Chandrsuda, C. and Bradshaw, P., "Turbulence Structure of a Reattaching Mixing Layer," Journal of Fluid Mechanics, Vol. 110, 1981, pp. 171-194.

13. Hanjalic, K. and Launder, B. E., "A Reynolds Stress Model of Turbulence and Its Application to Thin Shear Flows," Journal of Fluid Mechanics, Vol. 52, Part 4, 1972, pp. 609-638.

14. Shir, C. C., "A Preliminary Numerical Study of Atmospheric Turbulent Flows in the Idealized Planetary Boundary Layer," Journal of Atmospheric Science, Vol. 30, 1973, pp. 1327-1339.

15. Cormack, D. E., Leal, L. G., and Seinfeld, J. H., "An Evaluation of Mean Reynolds Stress Turbulence Models: The Triple-Velocity Correlation," ASME Journal of Fluids Engineering, Vol. 100, 1978, pp. 47-54.

16. Amano, R. S., "Development of Turbulent Near-Wall Model and Its Application to Separated and Reattached Flows," Numerical Heat Transfer, Vol. 7, No. 1, 1984, pp. 59-75.

17. Smyth, R., "Turbulent Flow Over a Disk Normal to a Wall," ASME Journal of Fluids Engineering, Vol. 101, 1979, pp. 461-465.

7. FIGURES

Fig. 1. Cell structure.

Fig. 2. Computational domain for the disk flow.

Fig. 3 Computational domain for the step flow.

Fig. 4. Mean velocity profiles behind the disk.

Fig. 5. Reynolds-stress profiles behind the disk.

Fig. 6. Reynolds-stress profiles behind the disk.

Fig. 7. All the Reynolds stresses behind the disk.

Fig. 8. Mean velocity profiles behind the step.

Fig. 9. Reynolds-stress profiles beyond the step.

Fig. 10. Triple-velocity product profiles beyond the step (original models).

Fig. 11. Triple-velocity product profiles beyond the step (overall correction factors are used).

Fig. 12. Triple-velocity product profiles beyond the step (individual correction factors are used for each component).

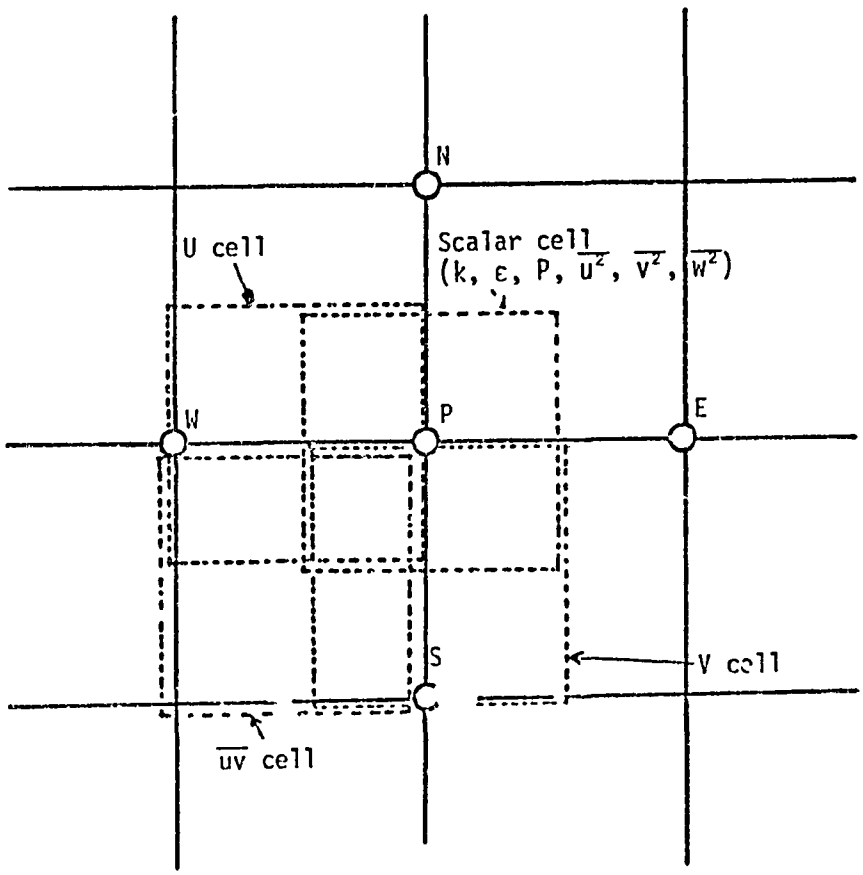

Figure 1 Cell structure.

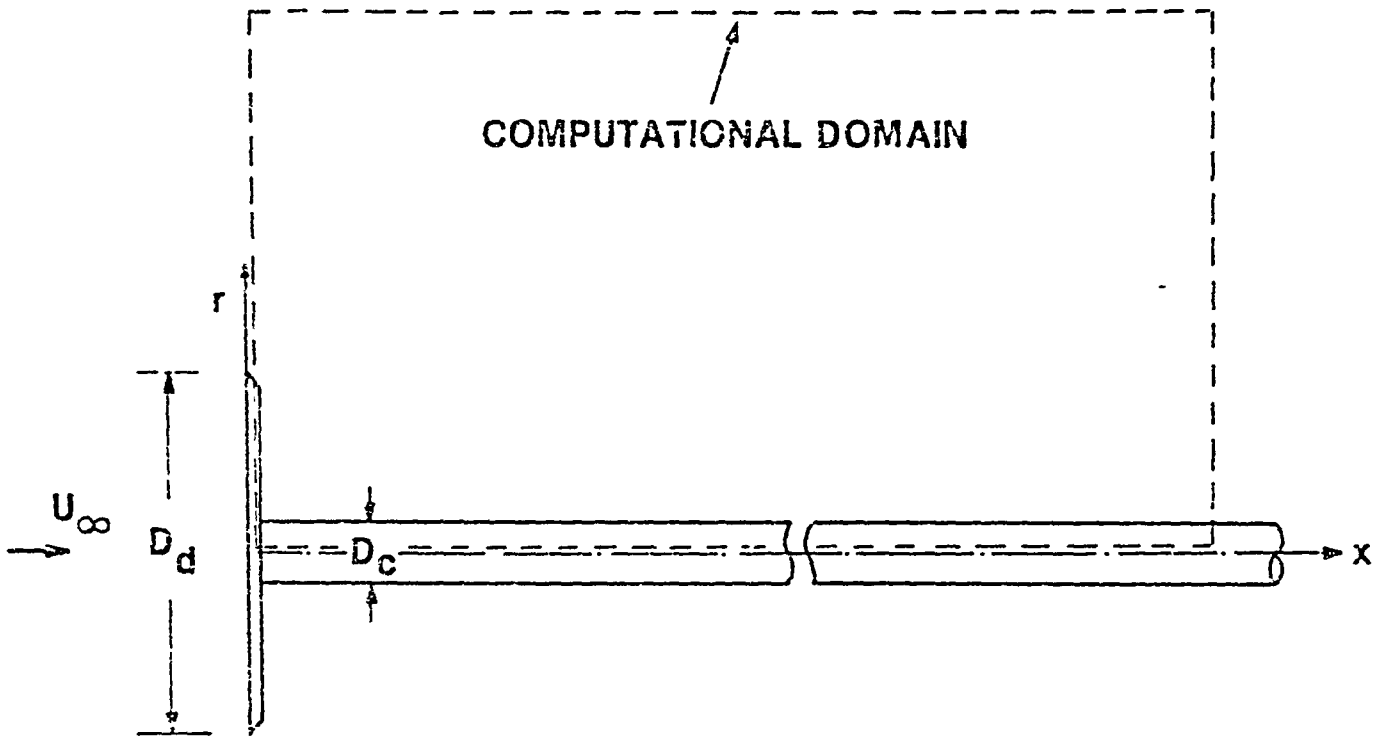

Fig. 2. Computational domain for the disk flow.

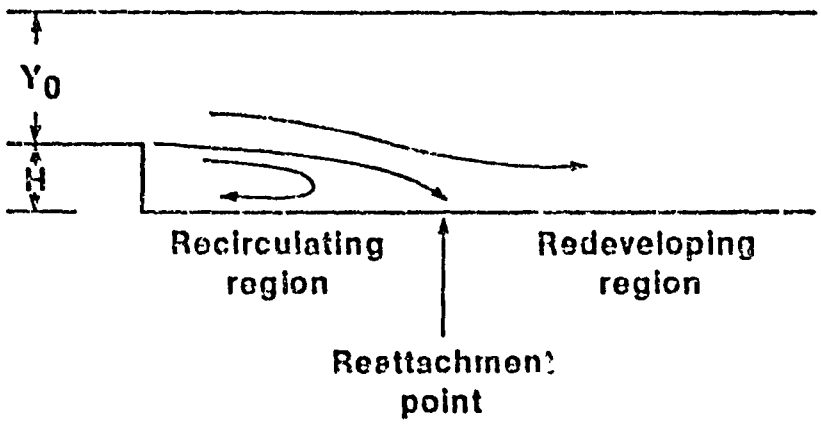

Fig. 3. Computational domain for the step flow.

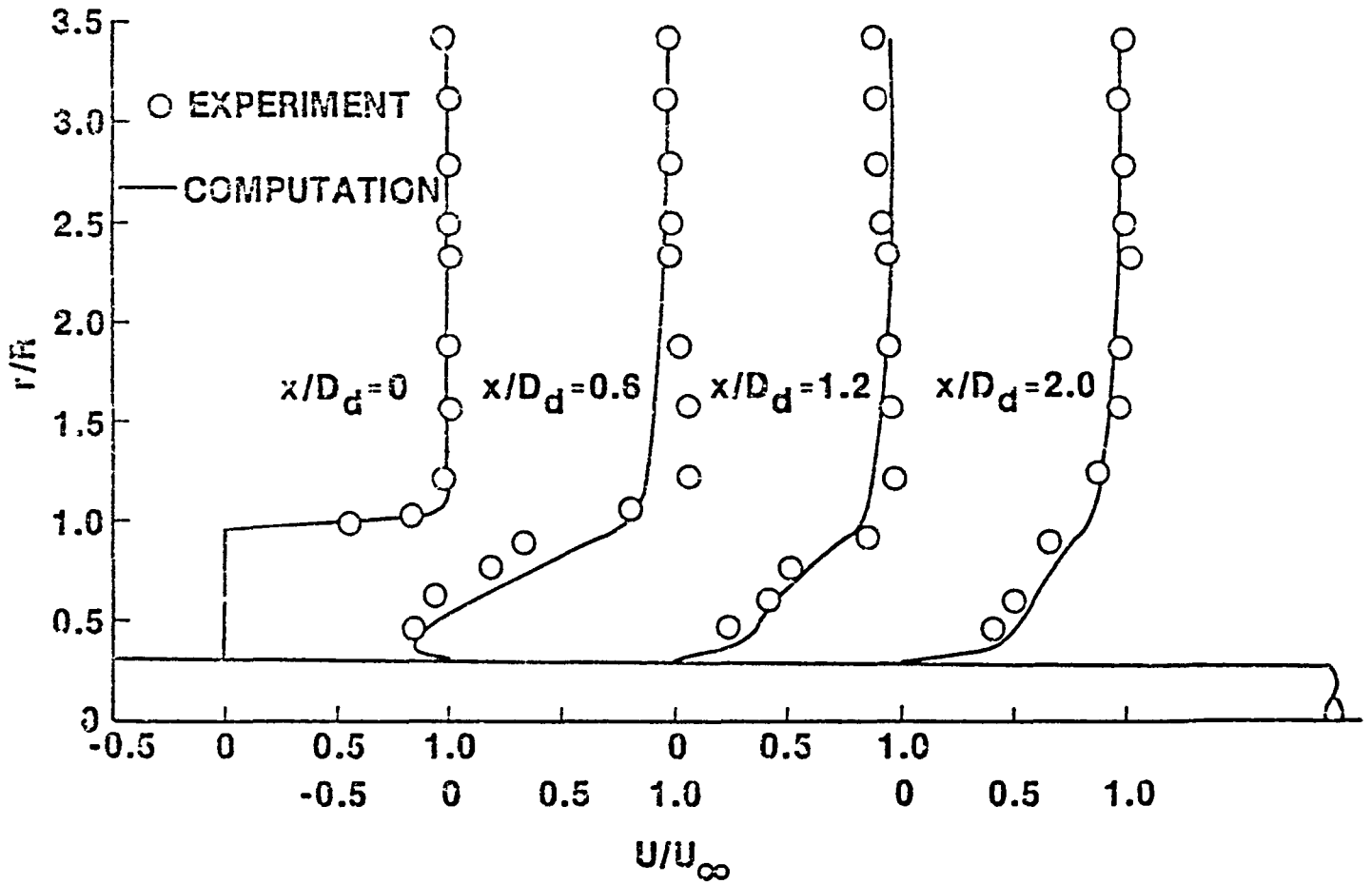

Fig. 4. Mean velocity profiles behind the disk.

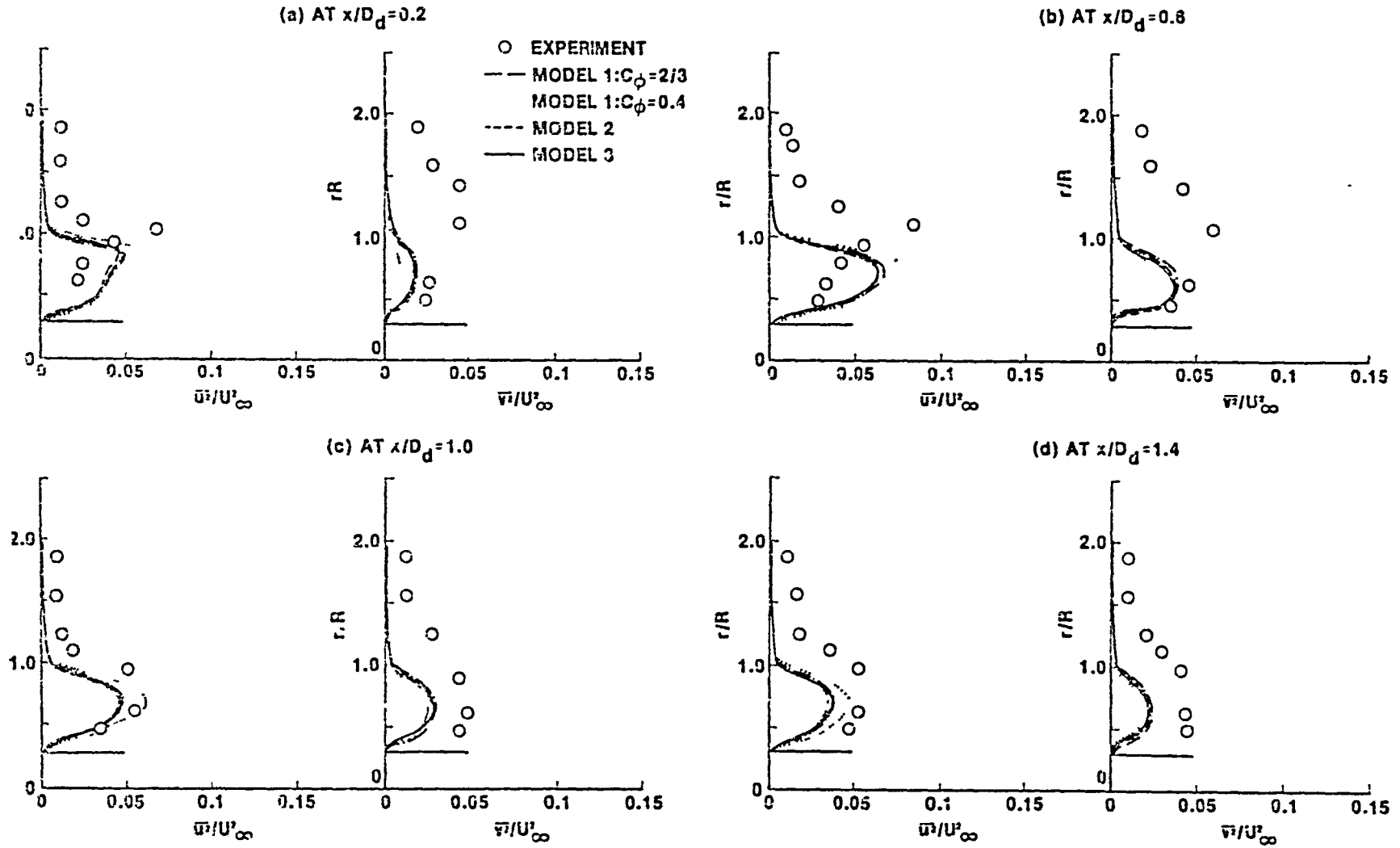

Fig. 5. Reynolds-stress profiles behind the disk.

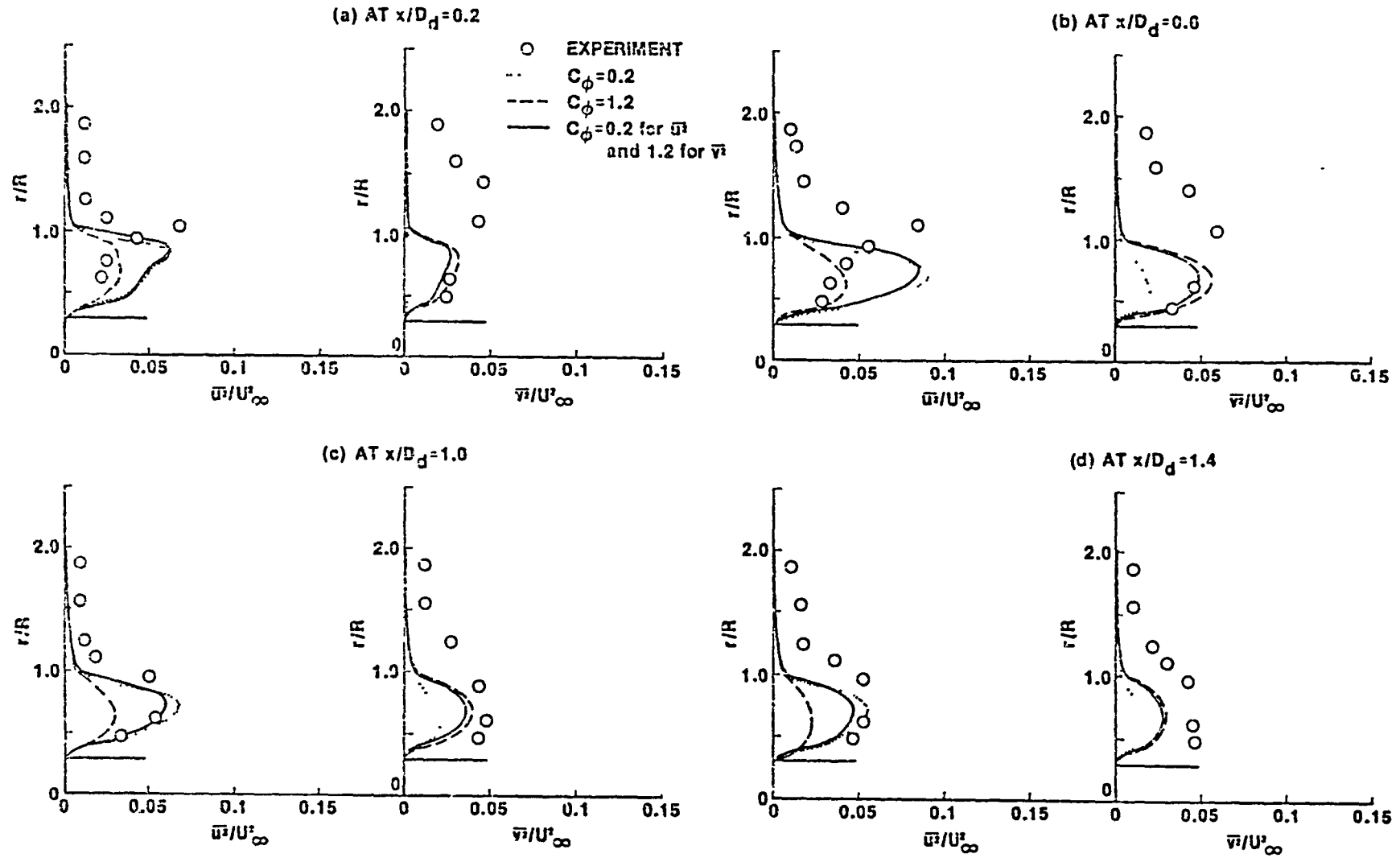

Fig. 6. Reynolds-stress profiles behind the disk.

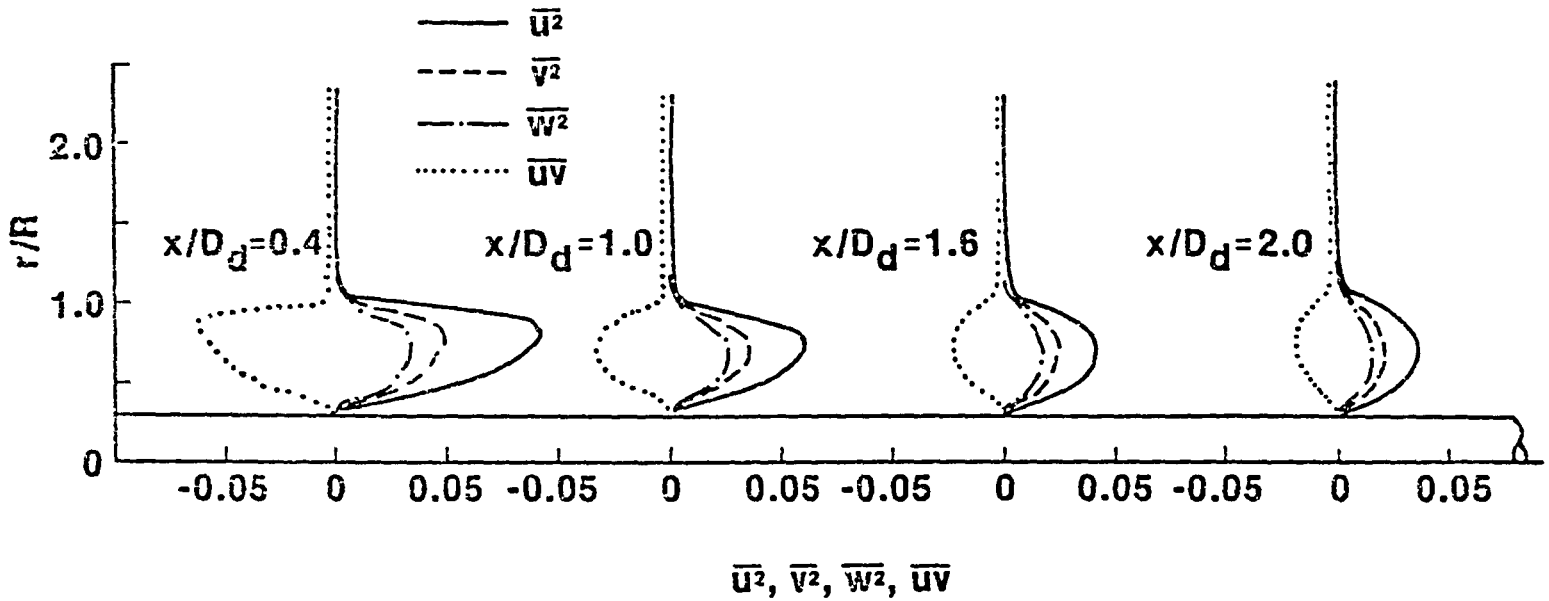

Fig. 7. All the Reynolds stresses behind the disk.

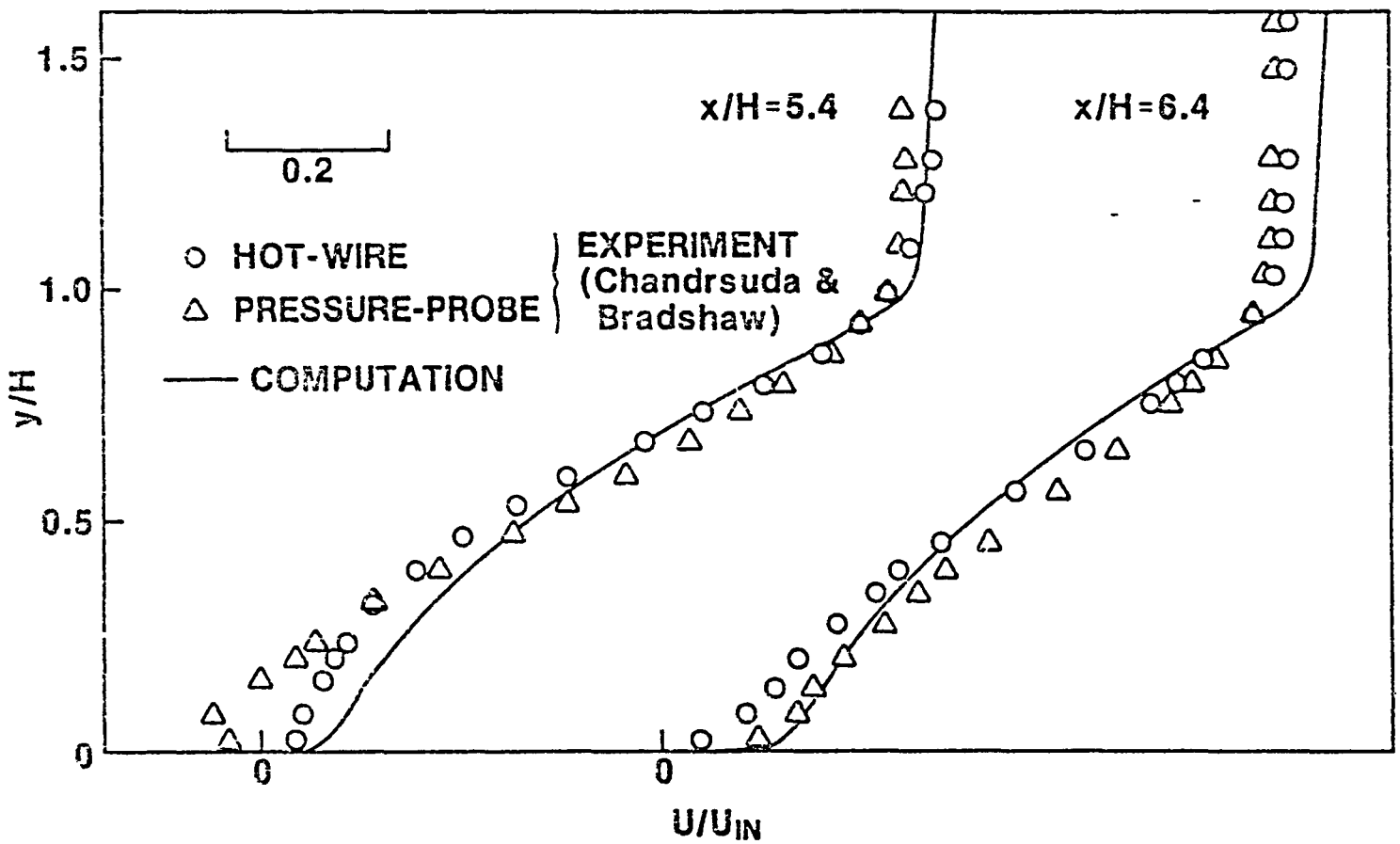

Fig. 8. Mean velocity profiles behind the step.

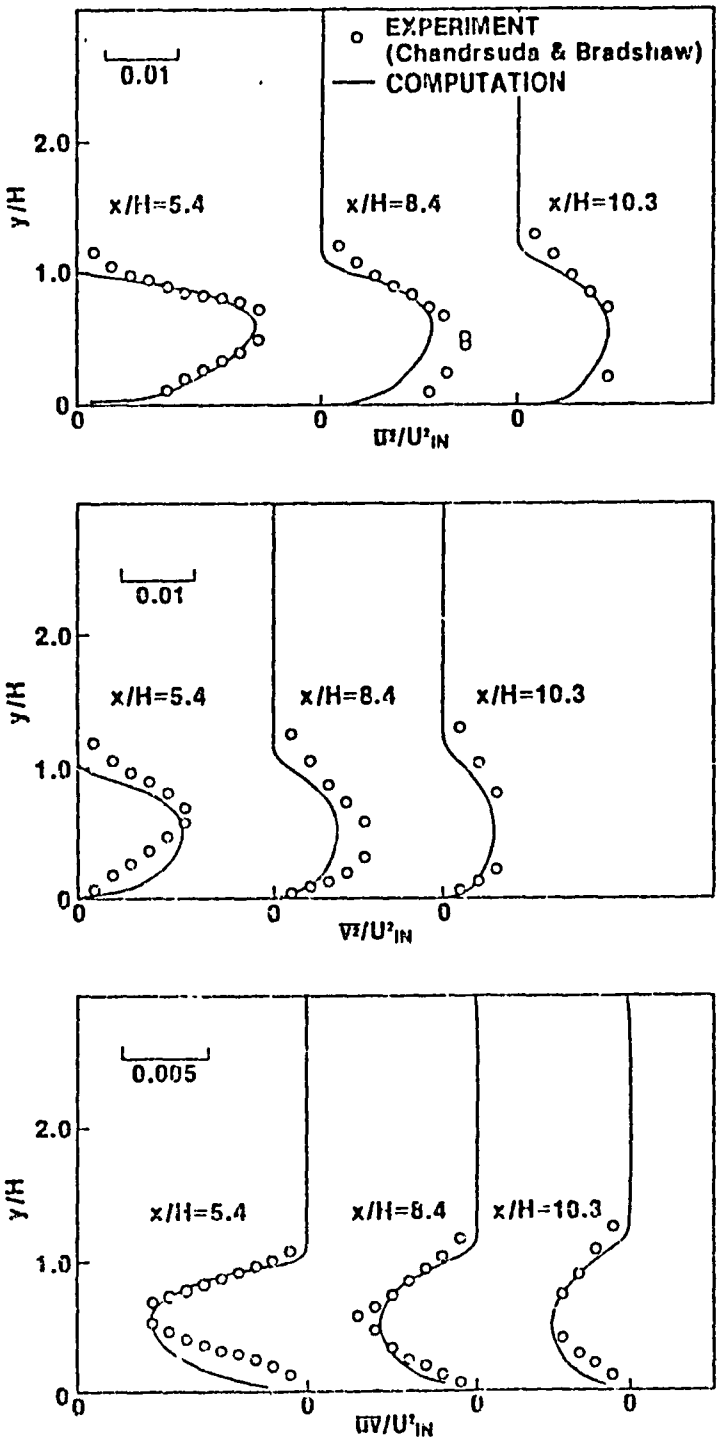

Fig. 9. Reynolds-stress profiles beyond the step.

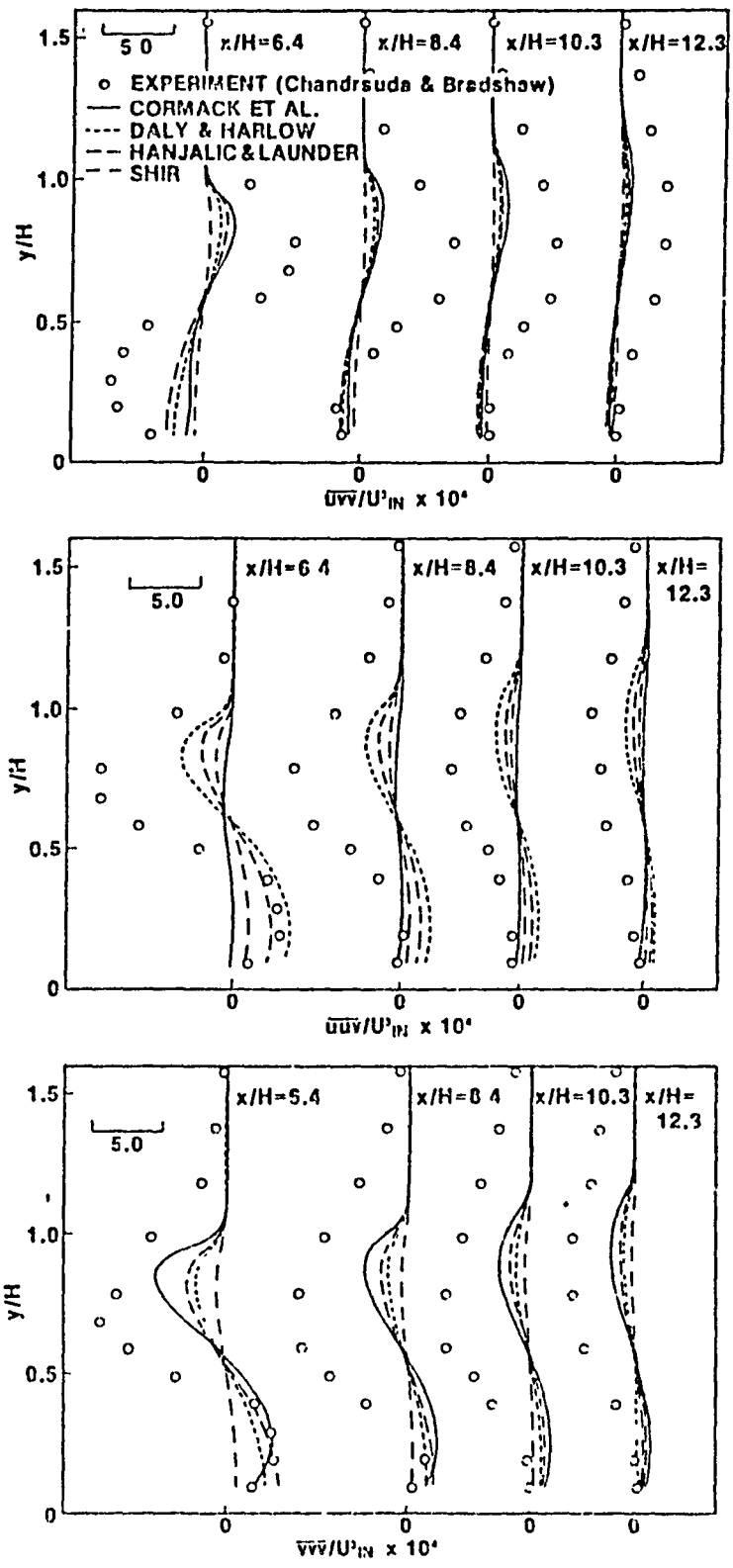

Fig. 10. Triple-velocity product profiles beyond the step (original models).

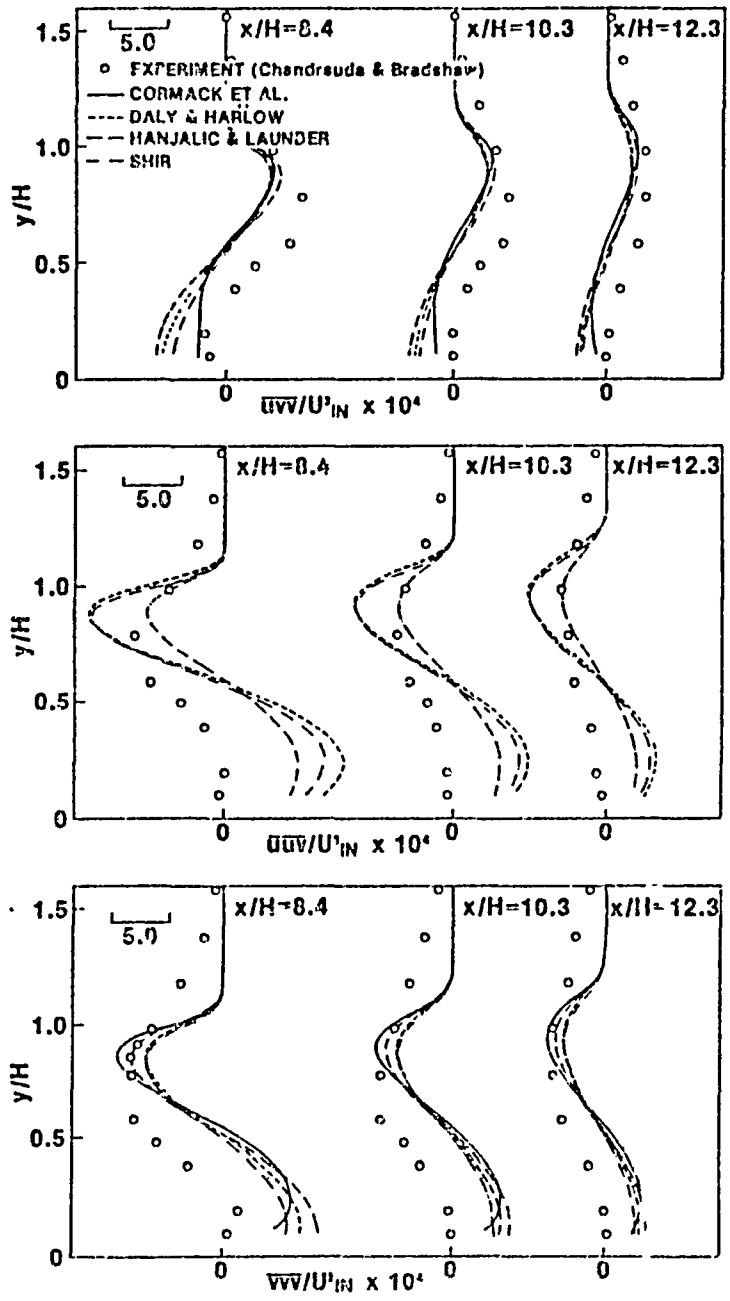

Fig. 11. Triple-velocity product profiles beyond the step (overall correction factors are used).

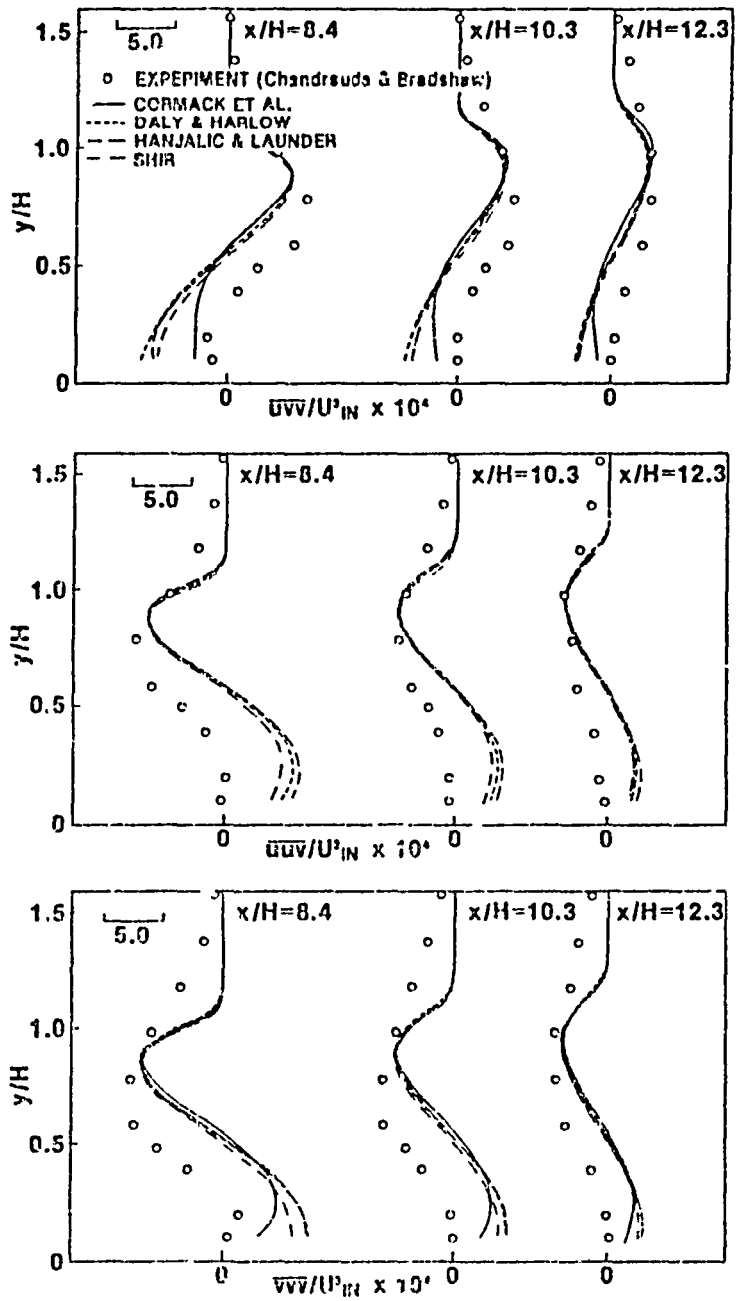

Fig. 12. Triple-velocity product profiles beyond the step (individual correction factors are used for each component).

END

DATE

FILMED

NOV 6 1986

End of Document